Expected Performances of the Copernicus Imaging Microwave Radiometer (CIMR) for an All-Weather and High Spatial Resolution Estimation of Ocean and Sea Ice Parameters

Lise Kilic, Catherine Prigent, Filipe Aires, Jacqueline Boutin, Georg Heygster, Rasmus T Tonboe, Fabien Roquet, Carlos Jimenez, Craig Donlon

Journal of Geophysical Research: Oceans

RESEARCH ARTICLE
10.1029/2018JC014408

Expected Performances of the Copernicus Imaging Microwave Radiometer (CIMR) for an All-Weather and High Spatial Resolution Estimation of Ocean and Sea Ice Parameters

Lise Kilic[1], Catherine Prigent[1,2], Filipe Aires[1,2], Jacqueline Boutin[3], Georg Heygster[4], Rasmus T. Tonboe[5], Hervé Roquet[6], Carlos Jimenez[1,2], and Craig Donlon[7]

[1]Sorbonne Université, Observatoire de Paris, Université PSL, CNRS, LERMA, Paris, France, [2]Estellus, Paris, France, [3]Sorbonne Université, CNRS, IRD, MNHN, LOCEAN, Paris, France, [4]Institute of Environmental Physics, University of Bremen, Bremen, Germany, [5]Danish Meteorological Institute, Copenhagen, Denmark, [6]Météo-France, Lannion, France, [7]European Space Agency, ESTEC, Noordwijk, The Netherlands

Abstract Climate change resulting in ocean warming, sea level rise, and sea ice melting has consequences for the global economy, navigation, and security. The Copernicus Imaging Microwave Radiometer (CIMR) mission is a high priority candidate mission within the European Copernicus Expansion program. CIMR is designed to observe the ocean and sea ice and more particularly the Arctic environment. Sea surface temperature (SST), ocean wind speed, sea surface salinity (SSS), and sea ice concentration (SIC) are fundamental variables for understanding, monitoring, and predicting the state of the ocean and sea ice. CIMR is a conically scanning microwave radiometer imager that includes channels at 1.4, 6.9, 10.65, 18.7, and 36.5 GHz, in a Sun-synchronous polar orbit, to provide SST, ocean wind speed, SSS, and SIC with an increased accuracy and/or spatial resolution. Here we analyze the performances of the CIMR mission in terms of theoretical retrieval precision and spatial resolution on the SST, SSS, and SIC products. A careful information content analysis is conducted. The CIMR performances are compared with the Advanced Microwave Scanning Radiometer 2 and the Soil Moisture Active Passive current missions. Maps of the retrieval precision based on realistic conditions are computed. CIMR will provide SST, SSS, and SIC with a spatial resolution of 15, 55, and 5 km and a precision of 0.2 K, 0.3 psu, and 5%, respectively. The SST and SIC will be retrieved at better than 30 km from the coast. CIMR is currently in preparatory phase, and if selected, it is for a launch in the 2025+ time frame.

Plain Language Summary Climate change resulting in ocean warming, sea level rise, and sea ice melting has consequences for the global economy, navigation, and security. The Copernicus Imaging Microwave Radiometer mission is a high priority candidate satellite mission within the European Copernicus Expansion program. It is designed to observe the ocean and sea ice and more particularly the Arctic environment. Sea surface temperature, ocean wind speed, sea surface salinity, and sea ice concentration are fundamental variables for understanding, monitoring, and predicting the state of the ocean and sea ice. Here we analyze the performances of this new satellite mission in terms of precision and spatial resolution on the sea surface temperature, sea surface salinity, and sea ice concentration and compare it with current missions. The Copernicus Imaging Microwave Radiometer will provide sea surface temperature, sea surface salinity, and sea ice concentration with a spatial resolution of 15, 55, and 5 km and a precision of 0.2 K, 0.3 psu, and 5%, respectively. This satellite mission is currently in preparatory phase, and if selected, it is for a launch in the 2025 time frame.

Key Points:
- A new passive microwave satellite mission is presented for high spatial resolution observations of polar regions
- An information content analysis is performed between 1.4 and 36.5 GHz for multiple ocean and sea ice parameters
- Sea surface temperature and sea ice concentration are retrieved respectively at 15 and 5 km with standard deviation errors of 0.2 K and 5%

Correspondence to:
L. Kilic,
lise.kilic@obspm.fr

Citation:
Kilic, L., Prigent, C., Aires, F., Boutin, J., Heygster, G., Tonboe, R. T. et al. (2018). Expected performances of the Copernicus Imaging Microwave Radiometer (CIMR) for an all-weather and high spatial resolution estimation of ocean and sea ice parameters. *Journal of Geophysical Research: Oceans*, *123*. https://doi.org/10.1029/2018JC014408

Received 26 JUL 2018
Accepted 27 SEP 2018
Accepted article online 4 OCT 2018

1. Introduction

Characterization of the ocean surface from Earth observation satellites is required to monitor, understand, and predict the state of the ocean and atmosphere and to study the energy and hydrological cycles. The oceans exchange with the atmosphere large amounts of heat, moisture, momentum, and gases. These exchanges vary at time scales from seconds (e.g., wave breaking), hours to days (e.g., storms), years (e.g., El Niño), and centuries (climate trends). The oceans have absorbed more than 90% of Earth heating due to the anthropogenic

increase in greenhouse gas concentrations over the last 50 years (Stocker et al., 2013), resulting in detectable ocean warming, land and sea ice melting, with consequences for sea level rise, the global economy, and security of life and property. Sea surface temperature (SST), ocean wind speed (OWS), sea surface salinity (SSS), and sea ice concentration (SIC) are fundamental variables for understanding, monitoring, and predicting the state of the ocean and atmosphere. They are required to correctly describe air/sea/ice interactions occurring at different scales, down to ocean submesoscale (Frenger et al., 2013; Perlin et al., 2014), and to drive the boundary condition of both Numerical Ocean Prediction and Weather Prediction models (Bell et al., 2000).

Copernicus (http://www.copernicus.eu/) is a European system for monitoring the Earth. It includes Earth observation satellites, ground-based measurements, and services to provide users with reliable and up-to-date information through a set of Copernicus Services related to environmental and security issues. The European Commission and the High Representative of the Union for Foreign Affairs and Security Policy issued to the European Parliament and the Council, on 27 April 2016, a joint communication that proposed *An integrated Europe Union policy for the Arctic*. The Arctics fragile environment is also a direct and key indicator of the climate change, which requires specific mitigation and adaptation actions, as agreed with the global agreement reached during COP-21 held in Paris in December 2015. The *integrated EU Arctic policy* has identified and is addressing three priority areas:

1. Climate Change and Safeguarding the Arctic Environment (livelihoods of indigenous peoples and Arctic environment).
2. Sustainable Development in and around the Arctic (exploitation of natural resources, e.g., fish, minerals, oil, and gas), Blue economy and safe and reliable navigation (e.g., the Arctic Northern Sea Route).
3. International Cooperation on Arctic Issues (scientific research, EU and bilateral cooperation projects, fisheries management/ecosystems protection, and commercial fishing).

Continuously monitoring the vast and harsh Arctic environment with Earth observation, navigation, and communication satellites is considered essential. The European Commission has expressed user needs in Duchossois et al. (2018a, 2018b) that recommends, as a first priority, an Imaging Microwave Radiometry Mission to address the Integrated EU Arctic Policy through the provision of operational ocean and sea-ice products with high spatial resolution, radiometric fidelity, and at least daily revisit in Polar regions. The Copernicus Imaging Microwave Radiometer (CIMR) mission is one of six High Priority Candidate Missions within the Copernicus Expansion programme focused on new missions that have been identified by the European Commission as priorities for implementation in the coming years to provide additional capabilities in support of high priority user needs. A full description of Mission Requirements for the CIMR mission are captured in Donlon (2018). The CIMR mission is currently in a phase A/B1 study expected to move into full implementation for a launch in the 2025+ time frame.

Global-scale measurements of ocean and sea ice variables such as SST and SIC can be derived from visible and infrared satellite observations. However, the temporal sampling of the visible and infrared observations is problematic especially over polar or tropical regions with very persistent cloud cover because at these wavelengths, clouds prevent a measurement of the ocean surface. More than 70% of the Earth surface is obscured by cloud at any time on average over the globe (Chelton & Wentz, 2005) with a particular challenge in the Tropical and Polar regions. Low-frequency passive microwave measurements between 1.4 and 37 GHz provide oceanic and sea ice variables such as SST, OWS, SSS, and SIC even under cloudy conditions and at night. Between 4 and 8 GHz, the passive microwave observations over open ocean are proportional to the SST within the first 1 mm of the surface. The signal is also sensitive to the OWS, with sea roughness being induced by the wind stress and the presence of foam at the sea surface. Above 3 GHz, sensitivity to SSS is very limited. Up to 12 GHz, the signal is also little affected by atmosphere (gas, clouds, and aerosols), except under rainy conditions. SST and OWS retrievals from satellite passive microwave sensors have been available since 1978, with dual polarization channels at 6.6, 10.7, 18, 21, and 37 GHz from the Scanning Multi-channel Microwave Radiometer. It was followed by the Tropical Rainfall Measuring Mission Microwave Imager, the Global Precipitation Measurement Microwave Imager, the WindSat polarimetric radiometer, the Advanced Microwave Scanning Radiometer for Earth Observing System (AMSR-E), and now the Advanced Microwave Scanning Radiometer 2 (AMSR2; ~50-km spatial resolution for the SST estimate). SST is produced with precision of the order of about 0.4 K (Gentemann et al., 2010; Nielsen-Englyst et al., 2018; Wentz et al., 2000), as compared to IR (0.16 K) or in situ measurements (0.23 K; O'Carroll et al., 2008). Microwave radiometer SSTs are routinely and operationally merged with IR observations (e.g., the UK Met Office OSTIA, Donlon et al., 2012; the Canada Meteorologi-

Table 1
The CIMR Instrument Requirements with a 7-m Diameter Antenna, as Compared to the Characteristics of Current Instruments With Real Aperture Antennas

Instrument	Frequency (GHz)	Spatial resolution (km)	Incidence angle (°)	NeΔT* (K)
CIMR	1.4	55	55	0.3
CIMR	6.9	15	55	0.2
CIMR	10.65	15	55	0.3
CIMR	18.7	5	55	0.3
CIMR	36.5	5	55	0.7
SMAP	1.4	40	40	0.93
AMSR2	6.9	48	55	0.3
AMSR2	7.3	48	55	0.3
AMSR2	10.65	33	55	0.6
AMSR2	18.7	18	55	0.6
AMSR2	23.8	14	55	0.6
AMSR2	36.5	9	55	0.6
AMSR2	89.0	4	55	1.1

Note. CIMR = Copernicus Imaging Microwave Radiometer; SMAP = Soil Moisture Active and Passive; AMSR2 = Advanced Microwave Scanning Radiometer 2.
*CIMR and SMAP have fore and aft looks. The averaging of these two looks leads to divide by $\sqrt{2}$ the instrument noise indicated in this table for these two instruments.

cal Center products, Meissner et al., 2016; and the JPL SST products, Chin et al., 2017). The remotely sensed OWS are primarily derived from scatterometer observations (i.e., active microwave observations), but the dual polarization microwave radiometer measurements also provide valuable wind speed estimates, especially at high wind speed (above ~15 m/s; Reul et al., 2017) where scatterometer measurements tend to saturate (Quilfen et al., 2007). SSS estimates have only been possible since the advent of satellite L-band measurements (1.4 GHz) from the Soil Moisture and Ocean Salinity mission (SMOS; since 2009), Aquarius, and now the Soil Moisture Active and Passive mission (SMAP; Boutin et al., 2016; Fore et al., 2016; Kao et al., 2018; Lagerloef et al., 2008; Le Vine et al., 2015; Meissner et al., 2018; Reul et al., 2014). When averaged over 1 week, the precision on the satellite salinity over the open ocean is typically 0.2 psu (Boutin et al., 2018).

Microwave radiometer sensors have been particularly successful for SIC mapping because, at these frequencies, microwaves are independent of daylight conditions, penetrate through clouds, and because of the very large brightness temperature (TB) contrast between sea ice and open water (up to 150 K at 6.9-GHz horizontal polarization; Ivanova et al., 2015). The North Pole is dark during 6 months of the year, and cloud cover is abundant (60–90%) in the Arctic region (Schweiger, 2004). The SIC has been retrieved with satellite microwave radiometer data since the 1970s, and the daily estimates of the global sea ice area and extent from these data are one of the longest continuous climate records (Stocker et al., 2013; Tonboe et al., 2016). Microwave frequency channels spanning from 1 to nearly 100 GHz are used for SIC retrieval (Gabarro et al., 2017; Ivanova et al., 2015). Recently, in an evaluation of over 20 different SIC algorithms (not including L band), it was found that the algorithm using 6.9-GHz data had the lowest noise level of all the algorithms (Ivanova et al., 2015). This is because the 6.9-GHz data are affected less by atmospheric and snow cover absorption and scattering variability than the higher frequencies. However, the spatial resolution at 6.9 GHz, with current and past missions, is very coarse compared to higher frequencies (see Table 1), and when retrieving SIC with current and past microwave radiometers, it is a trade-off between high spatial resolution and low SIC noise.

Current satellite microwave radiometer observations are limited in their application due to their poor spatial resolution at the low frequencies (~32 × 64 km at 6.9 GHz), with the related contamination in the coastal region and marginal ice zones. The mesoscale to submesoscale variabilities of the products are not captured, and within several tenths of kilometers from the coast or sea ice margin, the retrievals are contaminated. In addition, there is no guarantee today of the continuation of microwave radiometer measurements at low

frequencies, neither at 6.9 and 10.65 GHz after AMSR2 (Imaoka et al., 2010) nor at 1.4 GHz after SMOS and SMAP. In the context of CIMR, this is a primary challenge to address.

Here we analyze the potential baseline version of the CIMR conically scanning microwave radiometer imager that includes channels between 1.4 and 36.5 GHz, in a Sun-synchronous polar orbit, to provide SST, OWS, SSS, and SIC with an increased accuracy and spatial resolution compared to current products. The initial design included low-noise dual polarization receivers and a large 7-m rotating mesh antenna. Preliminary technical evaluations (Orlhac, 2012; Prigent et al., 2013) have been recently reconsidered, for ESA Earth Explorer projects. They showed that such a mission could be realistically equipped with a foldable antenna of the order of 7 m in diameter and low-noise receivers at 1.4, 6.9, 10.65, 18.7, and 36.5 GHz (L, C, X, Ku, and Ka bands). The channel requirements of such a mission (European Space Agency, 2018) are presented in Table 1, for an incidence angle of 55° and an orbit at 830 km as established during the studies related to the ESA Earth Explorer projects. They are compared to the characteristics of similar current instruments. Such a mission can completely cover the poles (no hole at the poles such as with classic polar orbiters). It is expected to fly in tandem with Meteorological Operational - Second Generation B (MetOp-SG B) to cover the full microwave spectrum from 1.4 to 664 GHz for the first time, by complementing the MetOp-SG B MicroWave Imager (between 18 and 190 GHz) and the Ice Cloud Imager (from 180 to 664 GHz).

The possible performances of the CIMR mission will be compared to current microwave satellite missions, in terms of geophysical product precision and spatial resolution. We will focus on the estimation of the SST, SSS, and SIC. The OWS will also be derived but mostly to correct the SST estimate from the roughness effect induced by wind stress, as the surface wind speed is better estimated from scatterometer observations for wind speeds of up to 25 m/s. Section 2 presents the methodology developed to estimate the retrieval precision for both ice-free and sea ice parameters. In section 3, retrieval precision maps are compared between the current missions and the CIMR mission. The important improvement for the coastal and sea-ice margin issue is also discussed. Section 4 concludes this study. The potential of a CIMR mission for other applications, including continental surface studies, is briefly discussed.

2. Estimation of the Retrieval Precision

2.1. An Information Content Analysis

To estimate the information content of the CIMR mission, we use a classical information content analysis (Rodgers, 1976, 1990). Similar methodology has been adopted in Prigent et al. (2013) for a limited number of channels and geophysical parameters; it was described in details therein.

The covariance matrix of the inversion error Q is expressed as

$$Q = (A^t \cdot S_\epsilon^{-1} \cdot A + S_f^{-1})^{-1}, \quad (1)$$

where A is the Jacobian matrix, S_ϵ is the observation error covariance matrix including the instrument and the forward model errors ($S_\epsilon = S_{\text{inst}} + S_{\text{FM}}$), and S_f is the covariance matrix of the first guess errors.

First, the Jacobian matrix A has to be estimated. Its dimension is the number of channels used in the retrieval multiplied by the number of parameters to be estimated. Its elements are the Jacobians of the TBs for the considered channels and parameters, that is, the derivative of the TB at the considered frequency, with respect to the parameter to be estimated. The covariance matrix of the instrumental noise (S_{inst}) is extracted from Table 1. The covariance matrix of the first guess error (S_f) corresponds to the error of the a priori information, before the inversion.

The square root of the Q matrix gives the theoretical retrieval error Standard Deviation (StD). The bias, that is, the systematic uncertainty, is not taken into account here; only the theoretical precision of the retrieval is estimated as always in this type of analysis. We are aware that additional errors can come from calibration and/or model uncertainties.

The retrieval error StD will be estimated separately for the ice-free ocean and sea ice parameters. Over ocean, physically based emissivity models have been developed and can provide reliable Jacobian calculations. Over sea ice, the emissivity models are not mature enough, and an alternative solution is proposed.

2.2. Precision Estimates for the Ice-Free Ocean Parameters

The ocean emissivity varies primarily with the OWS, the SST, and the SSS, with sensitivities that depend upon the frequency (Wilheit & Chang, 1980). The emissivity of a flat water surface can be calculated from the Fresnel equations for any incidence angle and orthogonal polarization, with the water permittivity calculated as

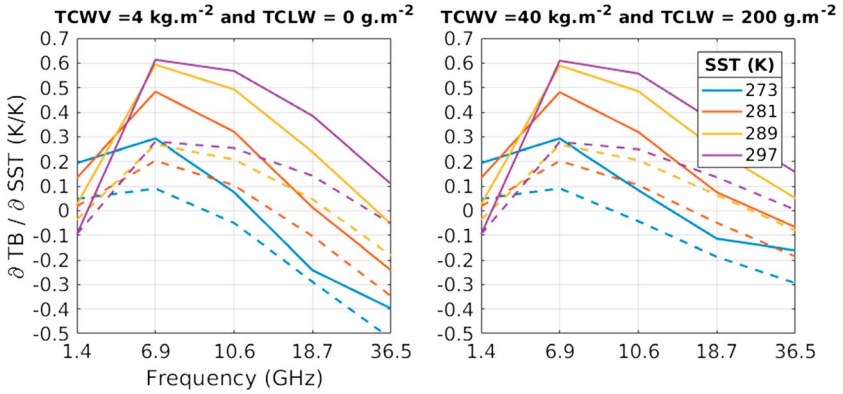

Figure 1. The SST Jacobians at the Copernicus Imaging Microwave Radiometer channels and at an incidence angle of 55° for different SSTs (colors), TCWV contents, and TCLW contents. Vertical and horizontal polarizations are, respectively, plotted as solid lines and dashed lines. The ocean wind speed is set at 6 m/s, and the SSS is set at 36 psu. SST = sea surface temperature; TB = brightness temperature; TCWV = Total Column Water Vapor; TCLW = Total Column Liquid Water.

a function of temperature and salinity. When the wind strengthens above the ocean, waves appear, and the surface is roughened. The large-scale waves can be treated as an ensemble of facets, for which Fresnel reflection applies, following geometric optics. The total emissivity is the sum of the contribution from each facet, weighted by the slope distribution. Small-scale roughness related to ripples has been added, and models include these two scales of roughness. In addition, above a certain wind speed, foam can appear. With an emissivity much higher than the water, the presence of foam can significantly modify the surface emissivity, through its coverage and emissivity.

We use the emissivity model developed by Dinnat et al. (2003) and Yin et al. (2012) at the Laboratory of Oceanography and Climate: Experiments and Numerical Approaches. It is based on the two-scale model of Yueh (1997), with a wave spectrum adapted from Durden and Vesecky (1985). The permittivity model of Klein and Swift (1977) is adopted, adjusted by Stogryn (1971). The foam cover from Yin et al. (2012) is selected along with the foam emissivity model from Stogryn (1972). This emissivity model is close to the model currently used for the operational processing of the SMOS data at 1.4 GHz, and we tested that it is relevant up to 37 GHz, as compared to an emissivity model such as FASTEM (Q. Liu et al., 2011) and AMSR2 satellite observations.

The atmospheric contribution to the signal is estimated using the community radiative transfer model RTTOV v12 (Saunders et al., 1999). It includes the water vapor absorption, as well as total liquid water radiative impacts.

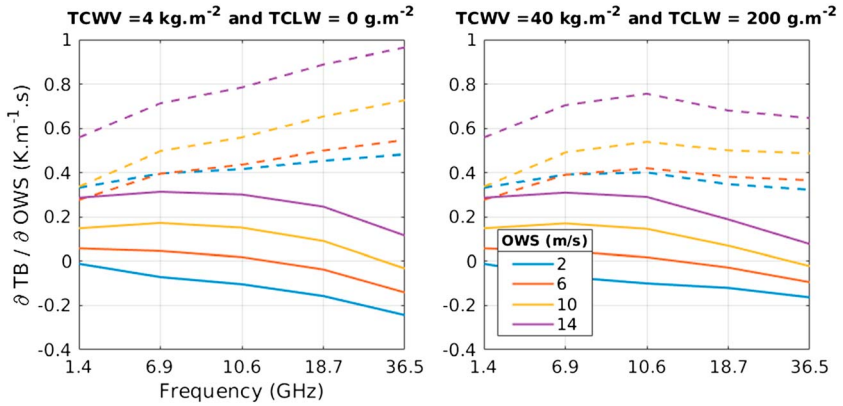

Figure 2. The OWS Jacobians at the Copernicus Imaging Microwave Radiometer channels and at an incidence angle of 55° for different OWSs (colors), TCWV contents, and TCLW contents. Vertical and horizontal polarizations are, respectively, plotted as solid lines and dashed lines. The SST is set at 285 K, and the SSS is set at 36 psu. OWS = ocean wind speed; TB = brightness temperature; TCWV = Total Column Water Vapor; TCLW = Total Column Liquid Water.

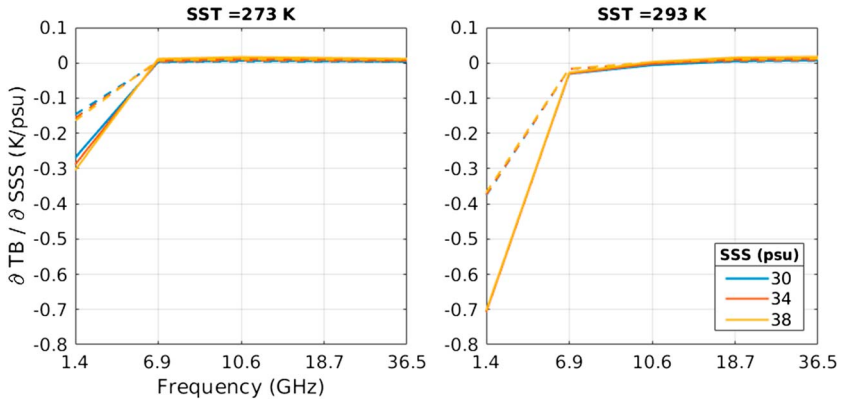

Figure 3. The SSS Jacobians at Copernicus Imaging Microwave Radiometer channels and at an incidence angle of 55° for different SSSs (colors) and SSTs (left to right). Vertical and horizontal polarizations are, respectively, plotted as solid lines and dashed lines. The ocean wind speed is set at 6 m/s; Total Column Water Vapor and Total Column Liquid Water are set to 0 kg/m^2. SST = sea surface temperature; SSS = sea surface salinity; TB = brightness temperature.

Over ice-free ocean, the sensitivity of the TB to the SST, OWS, and SSS is estimated under different surface and atmospheric conditions, for both orthogonal polarizations and for an incidence angle of 55°. The Jacobians are calculated using finite differences.

Figures 1 and 2 present the sensitivity of the sea TB to SST and OWS, under two Total Column Water Vapor contents (TCWV): a subarctic (4 kg/m^2) and a tropical (40 kg/m^2) atmospheres, and under two Total Column Liquid Water contents (TCLW): a clear sky (0 g/m^2) and a cloud with 200-g/m^2 liquid water. Note that an atmosphere with a TCLW content larger than ~200 g/m^2 is likely to precipitate. The sensitivity to the SST is higher at vertical than at horizontal polarization. The 6.9-GHz vertical polarization provides the best sensitivity (Figure 1), with little effect of the OWS (Figure 1) and the SSS (Figure 3). At 6.9 and 10.65 GHz, the sensitivity to SST increases with SST, with the consequence that the retrieval of the low SST will be more challenging than at higher SST. The effect of water vapor and cloud liquid water is limited up to ~10 GHz. It is observable at 18.7 GHz but still limited. At 36.5 GHz, the sensitivity to liquid water is important. The OWS Jacobian is higher for horizontal polarization, and it increases with frequency between 1.4 and 18.7 GHz under dry atmospheres. As for the SST, the impact of the water vapor and cloud liquid water is limited up to 10 GHz.

Figure 3 shows the sensitivity to SSS, for different SSSs and SSTs conditions. As expected, the 1.4-GHz sensitivity is the highest: it increases with SST, meaning that the retrieval of SSS is more difficult for low SST typical in the higher latitudes. We also investigated the sensitivity of the channels to the TCWV and the TCLW contents (Figure 4) showing limited sensitivity up to 10 GHz.

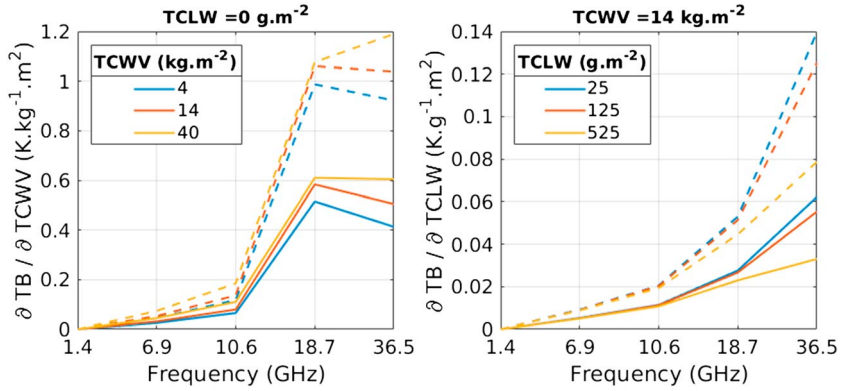

Figure 4. The TCWV (left) and the TCLW (right) Jacobians at Copernicus Imaging Microwave Radiometer channels and at an incidence angle of 55° for different TCWVs and TCLWs (colors), respectively. Vertical and horizontal polarizations are, respectively, plotted as solid lines and dashed lines. The sea surface temperature is set at 285 K, the ocean wind speed is set at 6 m/s, and the sea surface salinity is set at 36 psu. TCWV = Total Column Water Vapor; TCLW = Total Column Liquid Water; TB = brightness temperature.

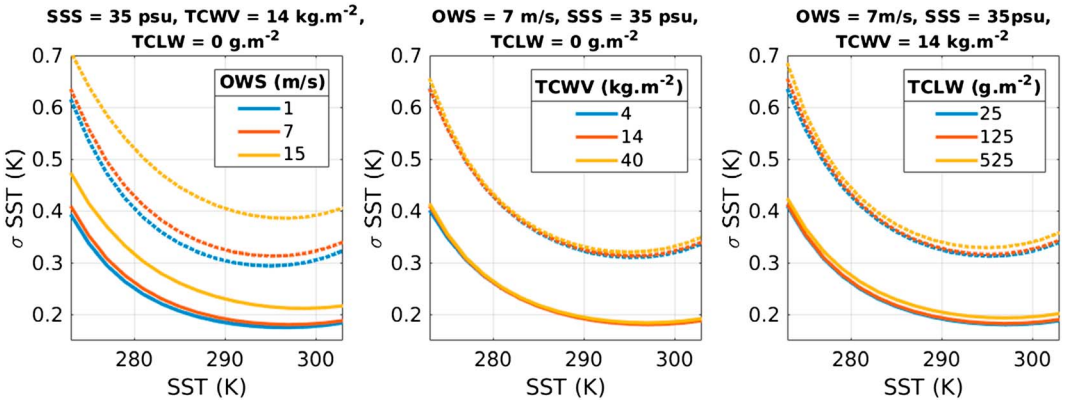

Figure 5. The SST theoretical retrieval error standard deviation estimated with the Copernicus Imaging Microwave Radiometer specifications (solid lines) and the Advanced Microwave Scanning Radiometer 2 specifications (dotted lines) for different OWSs (left), TCWVs (middle), and TCLWs (right). SST = sea surface temperature; OWS = ocean wind speed; SSS = sea surface salinity; TCWV = Total Column Water Vapor; TCLW = Total Column Liquid Water.

The covariance matrix Q of the retrieval error is computed for a given state (SST, SSS, OWS, TCWV, and TCLW). Following our previous study (Prigent et al., 2013), the first guess errors in S_f are 3.3 K for the SST, 1.3 m/s for OWS, 1 psu for the SSS, and 20% for TCWV as for TCLW. The two last a priori errors (TCWV and TCLW) are state dependent meaning that S_f in equation (1) is changed for each atmospheric situation. For the estimation of the retrieval precision of ice-free ocean parameters, we do not take into account the forward model error S_{FM}, only the instrumental noise S_{inst} is considered (Nielsen-Englyst et al., 2018; Pearson et al., 2018; Prigent et al., 2013). The resulting Q matrix is a 5×5 square matrix where the diagonal represents the variances of the error in SST, OWS, SSS, TCWV, and TCLW. By taking the square root of the diagonal terms, we obtain the theoretical retrieval error StD.

Note that here we assume that the TBs are free from Radio Frequencies Interferences which is steadily increasing as the number of communication and television broadcast satellites. Detection and mitigation of Radio Frequencies Interferences is a significant challenge for microwave radiometers at these low frequencies, and dedicated solutions are planned for CIMR using both onboard and ground-based processors. In addition, we assume that at 1.4 GHz, the extraterrestrial radiation (Galaxy, Sun, and Moon) is already accounted for, as well as the Faraday rotation in the atmosphere, using the appropriate ancillary data (Reul et al., 2008). These effects will likely add noise to the SSS retrieval, but great care will be exercise to minimize their impact. It is planned to measure the third Stokes component at 1.4 GHz to alleviate these effects, as proved efficient for the previous L-band missions.

Figures 5 and 6 represent the theoretical retrieval error StD on SST and OWS estimated using all the CIMR channels (1.4 to 36.5 GHz) and using all the AMSR2 channels (6.9 to 89 GHz), for different SST, OWS, TCWV and TCLW conditions. The theoretical retrieval error StD on SST strongly depends upon the SST and OWS conditions. At low OWS, the error is lower. The error decreases rapidly with SST: this is explained from Figure 1 where the sensitivity to SST increases with SST for channels at 6.9 and 10.65 GHz. At low SST, the error is much larger (~0.45 K for CIMR and ~0.7 K for AMSR2) than at high SST (~0.2 K for CIMR and ~0.35 K for AMSR2). The water vapor content does not impact the SST retrieval error StD. The impact of the liquid water content on the SST retrieval error is limited. The OWS retrieval error StD with CIMR is between 0.1 and 0.3 m/s for a range of OWS up to 15 m/s. Figure 7 represents the theoretical retrieval error StD on SSS, for different SST and OWS. The instantaneous retrieval error StD on SSS is between 0.25 and 0.6 psu with CIMR for SSS ≃35 psu. The SSS retrieval error StD decreases with increasing SSS, and it depends strongly upon the SST, with the error decreasing sharply with increasing SST. There is also a slight increase in retrieval error with increasing OWS.

The theoretical retrieval error StDs on SST, OWS, and SSS are largely improved with CIMR compared to AMSR2 or SMAP due to the low-noise receivers of CIMR. Our sensitivity analysis showed that the SST retrieval depends strongly on the 6.9-GHz channel. As a consequence, the spatial resolution of the SST retrieval will be assigned the spatial resolution of the 6.9 GHz. For the SSS, the 1.4 GHz is by far the dominant frequency in the retrieval, and the spatial resolution of the SSS retrieval is considered the spatial resolution of the 1.4-GHz channel.

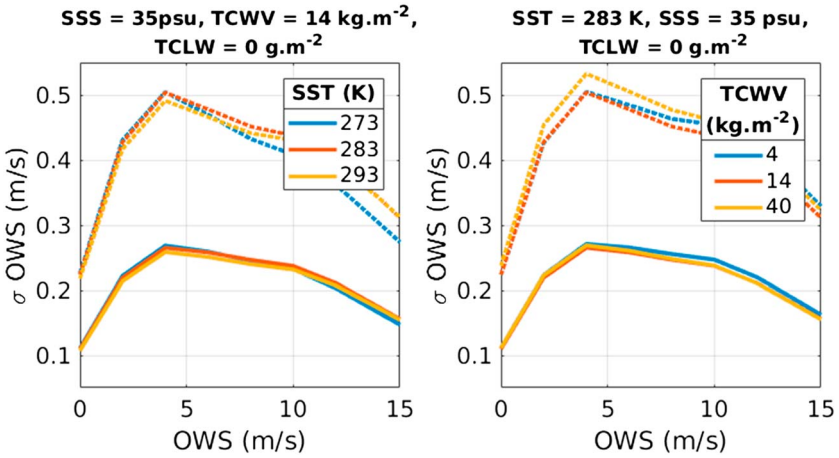

Figure 6. Theoretical retrieval error standard deviation of the OWS estimated with the Copernicus Imaging Microwave Radiometer specifications (solid lines) and the Advanced Microwave Scanning Radiometer 2 specifications (dotted lines) for different OWSs (left) and TCWVs (right). SST = sea surface temperature; OWS = ocean wind speed; SSS = sea surface salinity; TCWV = Total Column Water Vapor; TCLW = Total Column Liquid Water.

2.3. Precision Estimate for the Sea Ice Parameter

The sea ice is composed of different layers of ice, possibly covered by layers of snow. The sea ice emissivity at a certain polarization, frequency, and incidence angle is a function of subsurface extinction and reflections between layers with different permittivity. The sea ice permittivity and scattering are largely driven by the size and number density of brine pockets or air bubbles (Winebrenner et al., 1992). Snow cover is also very important for the signature variability of the sea ice types including multiyear ice and young ice (Eppler et al., 1992). Scattering in the snow pack is detectable for frequencies higher than ~10 GHz and is important for coarse snow grains or high frequency (>20 GHz). Sea ice emission models relate physical snow and ice properties such as density, temperature, snow crystal, and brine inclusion size to microwave attenuation, scattering, and reflectivity. Winebrenner et al. (1992) provide a review of different types of emission models that exist for sea ice. For example, the Microwave Emission Model for Layered Snow-packs is a model accounting for a detailed list of physical effects (Wiesmann & Mätzler, 1999). Microwave Emission Model for Layered Snow-packs has been extended to include emission from sea ice (Tonboe et al., 2006).

In practice, sea ice is a complex medium (including layering, differences in compaction and density, air bubbles, and brine pockets), and therefore, the simple models fail to simulate observations. In addition, Numerical

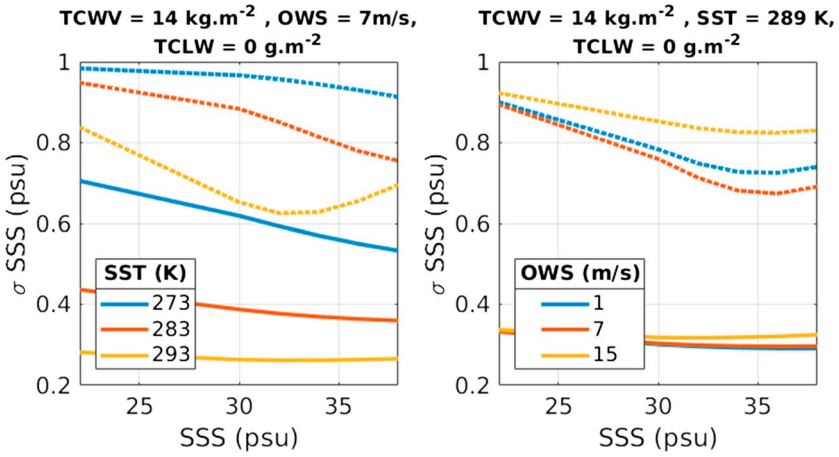

Figure 7. Theoretical retrieval error standard deviation of the SSS estimated with the Copernicus Imaging Microwave Radiometer specifications (solid lines) and the Soil Moisture Active and Passive radiometer specifications (dotted lines) for different SSTs (left) and OWSs (right). SST = sea surface temperature; OWS = ocean wind speed; SSS = sea surface salinity; TCWV = Total Column Water Vapor; TCLW = Total Column Liquid Water.

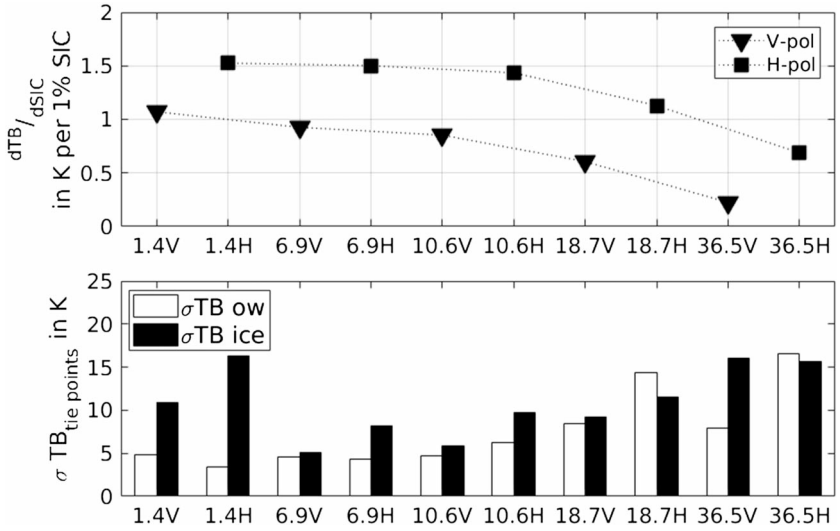

Figure 8. (top) Sensitivity of the TBs to SIC estimated from Round Robin Data Package from 1.4 to 36.5 GHz. (bottom) The TB standard deviations of the tie points (open water and sea ice) used to compute SIC from 1.4 to 36.5 GHz. TB = brightness temperature; SIC = sea ice concentration.

Weather Prediction models do not typically contain the parameters necessary to drive microwave emission models. Finally, the sea ice is dynamic: it drifts, deforms (ridging and lead opening), changes composition through time (brine rejection), melts, or reforms with possible significant changes from day-to-day.

Therefore, microwave SIC retrieval algorithms are based on empirical methods (e.g., Comiso et al., 1997; Markus & Cavalieri, 2000). The TB of sea ice is very large compared to that of ocean water, making the contrast very strong between these two states. Retrieval algorithms are derived from coincident data sets of satellite observations and in situ measurements, with fully ice covered sites (100% SIC) and purely open ocean areas (0% SIC), called tie points. Then, the forward model is a linear mixing approach of the TB contribution of the two surface types within the sensor footprint:

$$TB = SIC \times TB_{\mathrm{Ice}} + (1 - SIC) \times TB_{\mathrm{OW}}, \tag{2}$$

with TB_{Ice} the TB over 100% SIC and TB_{OW} the TB over Ocean Water (0% SIC). The error of the parametrization then depends on that of the tie points TB_{Ice} and TB_{OW}.

We use the forward model given in equation (2) to derive the expression of the sensitivity to SIC, that is, the TB variation from 100% to 0% SIC:

$$\frac{\mathrm{d}TB}{\mathrm{d}SIC} = TB_{\mathrm{Ice}} - TB_{\mathrm{OW}}. \tag{3}$$

To compute sensitivity to SIC, we use directly the difference of the ocean and sea ice TBs estimated from AMSR-E/AMSR2 and SMOS data in the Round Robin Data Package developed for the ESA sea ice Climate Change Initiative project (Pedersen & Saldo, 2016). The database totalizes 18,700 observations for areas with 0% SIC and 3,460 observations for areas with 100% SIC. The observation points are localized over Arctic and Antarctic for a period between 2010 and 2011. The mean values and the StDs of TB_{OW} and TB_{Ice} for the different channels are computed from this data set.

Figure 8 shows the sensitivity of the TBs measured by satellite to SIC (top) along with the StDs of the TBs of ocean water and sea ice (bottom) between 1.4 and 36.5 GHz. TB_{Ice} and TB_{OW} are used as tie points to compute SIC, and the error on their values directly impacts precision on SIC estimation. The sensitivity of the TBs to the SIC is very high compared to the sensitivity to SST, OWS, or SSS. We observe that the sensitivity to SIC decreases with frequency, and it is higher for the horizontal polarization than for the vertical polarization. The StDs of TB_{OW} and TB_{Ice} are larger for the horizontal polarization, especially for TB_{Ice}. Note that the 6.9-GHz vertical polarization channel has the lowest StD on the TBs of the tie points. The 1.4-GHz channels show a

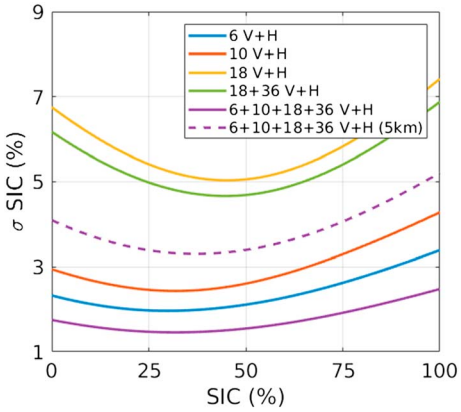

Figure 9. Theoretical retrieval error standard deviation on SIC from the information content analysis equation (5) with different combinations of Copernicus Imaging Microwave Radiometer channels. SIC = sea ice concentration.

good sensitivity to the SIC, actually larger than the 6.9 GHz. However, the 1.4-GHz emissivity presents a large variability over sea ice (likely due to some penetration in the subsurface and its sensitivity to sea ice thickness), and the channel has a low spatial resolution (limited by the size of the satellite instrument reflector). As a consequence, with the high requirement in spatial resolution for sea ice products, the 1.4 GHz will not be used in the SIC retrieval.

To evaluate the estimation of the sea ice retrieval error StD, the simple linear-mixing model for SIC is applied to all the channels from 6.9 to 36.5 GHz. In the information content analysis, equation (1): $S_f^{-1} = 0$ as there is no first guess in equation (2), and the instrumental noise S_{inst} is neglected in front of the forward model error S_{FM} in the observation error covariance matrix S_ε . The forward model error covariance matrix for the SIC retrieval is deduced from equation (2):

$$S_{\text{FM}} = SIC^2\sigma^2_{TB_{\text{Ice}}} + (1 - SIC)^2\sigma^2_{TB_{\text{OW}}}, \tag{4}$$

$\sigma^2_{TB_{\text{Ice}}}$ and $\sigma^2_{TB_{\text{OW}}}$ correspond, respectively, to the covariance matrix (here diagonal) of the TBs for 100% SIC and 0% SIC represented in Figure 8. As a consequence,

$$Q = \left(\left(\frac{\mathrm{d}TB}{\mathrm{d}SIC}\right)^t \times S_{\text{FM}}^{-1} \times \frac{\mathrm{d}TB}{\mathrm{d}SIC}\right)^{-1}. \tag{5}$$

Figure 9 shows the SIC retrieval error StD as a function of SIC, first for each frequency, using both vertical and horizontal polarizations. The calculations use the winter part of the Round Robin data set, as is usually done for model developments. The 6.9-GHz channels have the highest information content compared to the other channels. Note that the variability of the other geophysical parameters is already taken into account in the estimation error, as the TB_{Ice} and TB_{OW} variabilities in the database already include the variability of the environment (e.g., SST, TCWV, and TCLW). For the combination of the CIMR channels, each channel is taken at its nominal spatial resolution. The SIC product will be at the spatial resolution of the channel which drives the retrieval. The combined use of the 6.9-, 10.65-, 18.7-, and 36.5-GHz channels together improves the retrieval, with a SIC theoretical retrieval error StD between 2% and 3%.

Work is underway to develop a SIC retrieval method that benefits of the highest spatial resolution while using a combination of all available channels. Here we propose a preliminary estimate of the achievable SIC precision at 5 km, using together the 6.9-, 10.65-, 18.7-, and the 36.5-GHz channels. To account for the spatial resolution increase, the StDs of the tie points in the S_{FM} matrix of the channels with lower spatial resolution are multiplied by a factor of the channel resolution divided by the target resolution (15/5 at 6.9 and 10.65 GHz). The derived SIC retrieval error StD is plotted as a dashed line in Figure 9. The spatial resolution of the retrieval is improved to 5 km, but at the expense of a degraded precision on SIC, as expected. More work is to be done to refine this result and propose a robust and validated method to benefit from the frequency combination at high spatial resolution.

3. Performances of the Geophysical Product Retrieval With the CIMR Mission

3.1. Improved Spatial Resolution and Retrieval Precision: An Example Over North Atlantic

High latitudes and polar regions are particularly vulnerable to climate change. They are also cloud covered during large periods of the year. In these areas, improved all-weather, high spatial resolution, and accurate retrieval of the ocean and ice variables are particularly needed. Unfortunately, our previous information content analysis confirmed that the retrieval of ocean parameters (SST and SSS) is particularly difficult in these areas, with the sensitivity of the observations to these parameters decreasing with decreasing SST.

The performances of the CIMR mission are estimated in the North Atlantic area for SST, SSS, and SIC, in terms of retrieval precision and spatial resolution, as compared to the performances obtained with instruments such as AMSR2 and SMAP.

As already discussed, for the SST as well as for SIC, the retrieval is driven by the 6.9 GHz, and the spatial resolution of the SST and SIC products is limited by the spatial resolution of the 6.9-GHz channel. The design of the

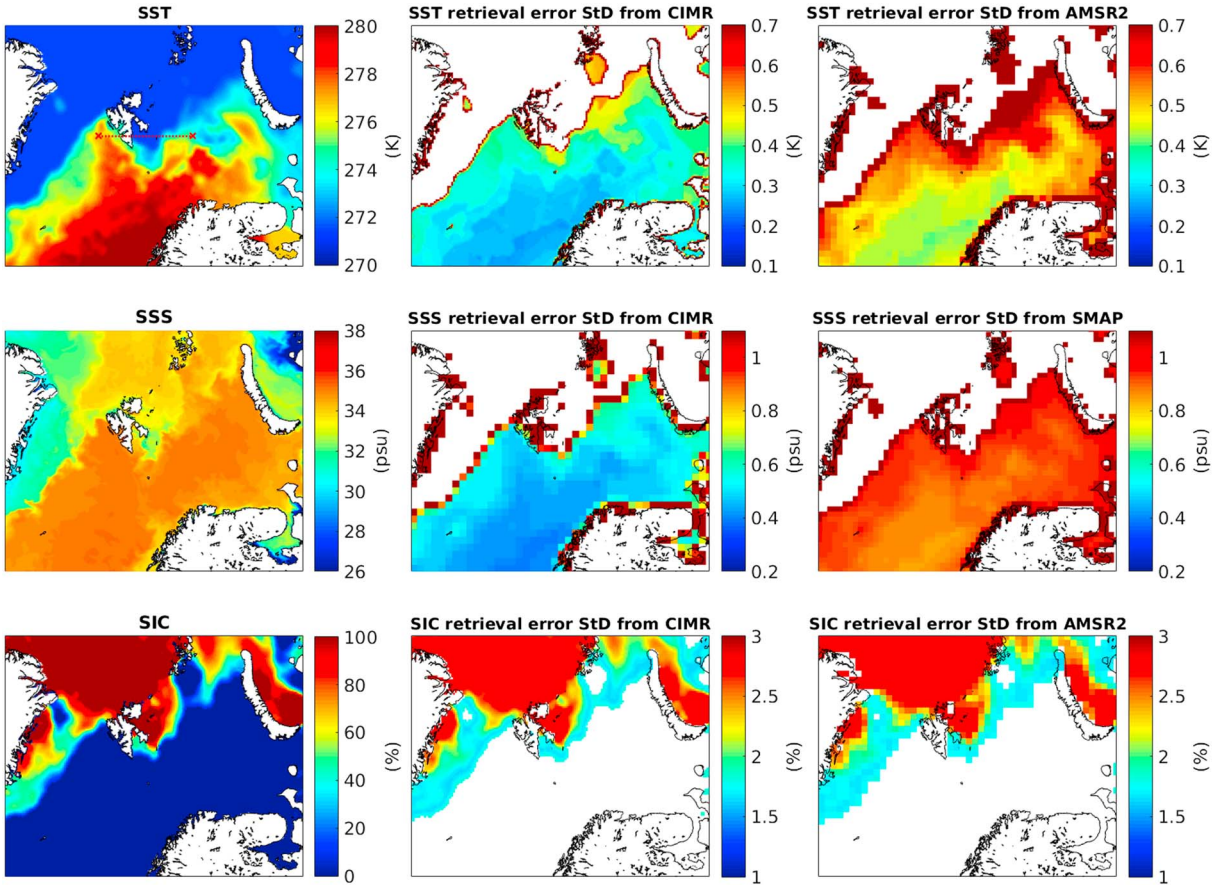

Figure 10. The SST, SSS, and SIC fields (first column) at 2-km resolution on 15 June 2008 and the theoretical retrieval error StD of the SST (top), the SSS (middle), and the SIC (bottom) for CIMR (second column) and for AMSR2 or SMAP (third column), as calculated from realistic sea and ice fields. A cross section close to the Spitzberg is indicated in red in the left top panel; it will be used to analyze further the coastal effect. SST = sea surface temperature; SIC = sea ice concentration; SSS = sea surface salinity; StD = standard deviation; CIMR = Copernicus Imaging Microwave Radiometer; AMSR2 = Advanced Microwave Scanning Radiometer 2; SMAP = Soil Moisture Active and Passive.

CIMR radiometer is taking particular care to minimize side-lobe contamination of all channels so that measurements will be useful within one spatial sampling distance of a boundary. The SSS estimate is essentially based on the observations at 1.4 GHz, and the spatial resolution of the SSS product corresponds to the spatial resolution at 1.4 GHz. Gaussian antenna patterns are assumed, with a half-power beam width corresponding to the spatial resolution.

A North Atlantic situation is selected on 15 June 2008. It includes sea ice cover and complex coastal effects. The oceanic and atmospheric fields at 2-km spatial resolution (SST, OWS, and SIC) are extracted from the HIgh Resolution Limited Area Model (HIRLAM) of the Norwegian Meteorological Institute for 1 day. The TCWV and the TCLW are provided by the European Centre for Medium-Range Weather Forecasts (ECMWF) interim Re-Analysis (ERA-interim) at 0.125° (~12 km) spatial resolution. The SSS fields are from the MERCATOR global forecast analysis at 0.083° (~8 km) spatial resolution. All the data fields are reprojected on the HIgh Resolution Limited Area Model grid.

For the maps of performances (Figures 10 and 12), the theoretical retrieval error StD is calculated for each pixel separately using the local environmental conditions. For SST calculations, the CIMR estimates (with channels 1.4 to 36.5 GHz) are compared to the AMSR2 estimates (with channels 6.9 to 89 GHz) with their respective noise from Table 1. For SSS calculations, the CIMR estimates (with channels 1.4 to 36.5 GHz) are compared to the SMAP estimates (with channels 1.4 GHz). For the SIC calculations, only the 6.9-, 10.65-, 18.7-, and 36.5-GHz channels are used for both CIMR and AMSR2.

For the retrieval error StD, the coastal or sea ice margin effects are also included, with an estimation of the bias errors related to the proportion of land and sea ice in the considered pixel, taking into account the spatial

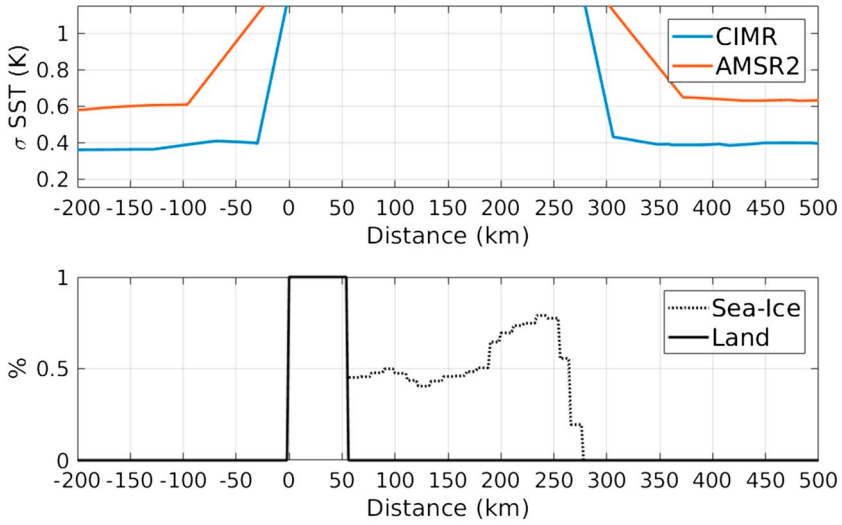

Figure 11. The theoretical retrieval error standard deviation on SST for CIMR and for AMSR2 along a transect close to Spitzberg (top) and the corresponding surface characteristics (bottom). The transect is indicated in the left top panel of Figure 10. SST = sea surface temperature; CIMR = Copernicus Imaging Microwave Radiometer; AMSR2 = Advanced Microwave Scanning Radiometer 2.

resolution of the different channels. Land and sea ice have large emissivities (close to unity) as compared to the ocean emissivity. The sea ice emissivity is considered at 0.98 (Gloersen et al., 1992; Markus & Cavalieri, 2004). The mode value of the land surface emissivity is close to 0.95, and this value is selected for our evaluation here. We are aware that land and sea-ice surface emissivity varies in space and time with surface properties (Aires et al., 2011; Prigent et al., 2006), but we present here a preliminary estimate of the coastal and ice margin effects. A first approximation of the error induced by land or/and sea-ice is calculated at the finer resolution of the simulation. Then the errors are averaged using the instrument field-of-view assuming Gaussian patterns; it results a map of the retrieval error StD with the spatial resolution of the given instrument and channel.

Figure 10 presents the surface SST, SSS, and SIC fields for 15 June 2008, with the theoretical retrieval errors on SST, SSS, and SIC obtained with CIMR and with the current missions (AMSR2 and SMAP). Major differences between the SST accuracy are related to the low instrument noise of CIMR, as compared to AMSR2. As expected from Figure 5, the retrieval precision degrades for low SST, closer to the colder waters of the high-latitude regions. For SIC, the instrument noise does not impact the retrieval because of the high dynamic range between open water and sea ice. The unique feature of CIMR for SIC retrieval is the improved spatial resolution. Using current instruments, to obtain such spatial resolution, higher microwave frequencies are used but with much stronger atmospheric contamination, as shown in the comparative study from Ivanova et al. (2015) where an experimental 6.9-GHz SIC retrieval based on AMSR-E observations performed best among 40 investigated algorithms. The spatial resolution of SSS from CIMR is coarser than the SMAP spatial resolution, but the precision of the estimate is improved, because of the lower noise figure of the 1.4-GHz channel of CIMR. As expected from Figure 7, the retrieval error StDs on SSS are larger for cold SSTs, closer to the poles.

A transect close to the Spitzberg is provided for a better quantification of the coastal and surface transition effects on the SST retrieval (Figure 11, with transect indicated in the left top panel of Figure 10). For AMSR2, the retrievals are affected by the surface transition (coast and sea ice for the ice-free ocean) as far as 100 km away from the transition zone. This distance reduces to less than 30 km with the CIMR spatial resolution (with a design target of 15–20 km). With the 6.9 GHz playing a major role in the retrieval of the SST, especially for low SST (Figure 1), the SST retrieval is likely to be affected as soon as the 6.9-GHz observation is contaminated by emissions entering through the antenna side lobes.

3.2. Performances at the Global Scale

The performance of the SST retrieval with CIMR is also evaluated at the global scale, using realistic surface and atmospheric fields. We use the SST and SIC produced daily on an operational basis at the UK Met Office with 0.054° spatial resolution (http://podaac.jpl.nasa.gov/dataset/UKMO-L4HRfnd-GLOB-OSTIA; Stark et al., 2007). They are complemented with the OWS, TCWV, and TCLW provided by the ECMWF ERA-Interim reanalysis at

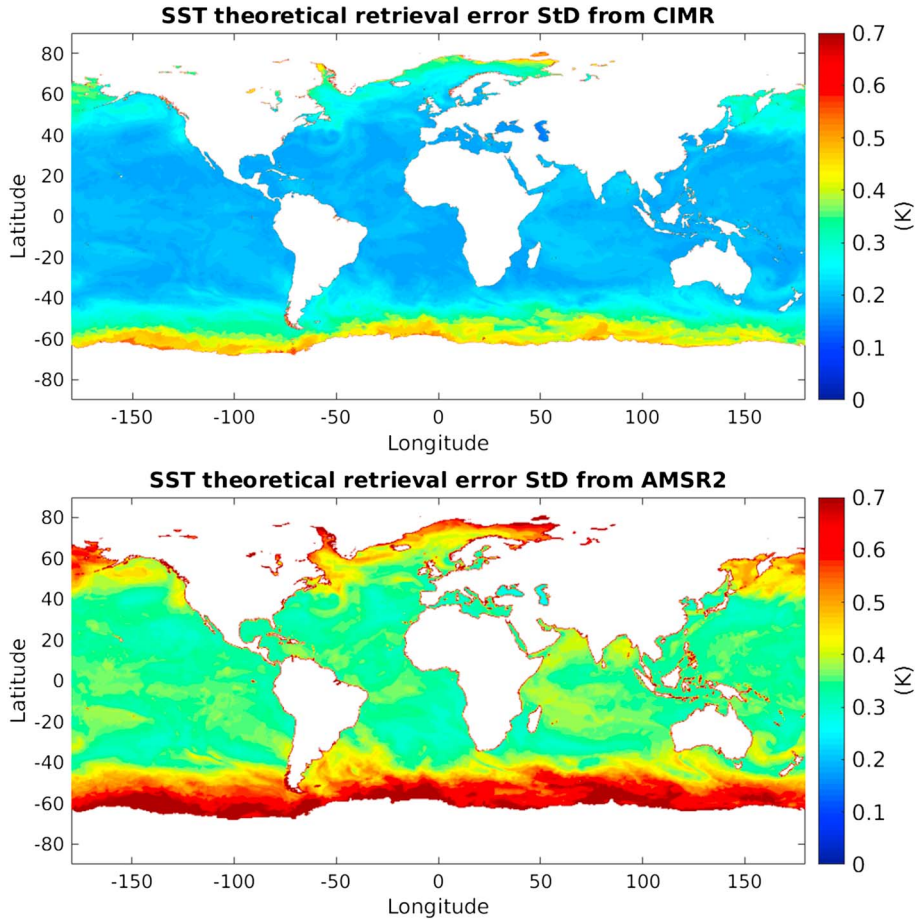

Figure 12. The theoretical retrieval error StD on SST for 1 day (15 June 2008) at global scale, estimated from radiative transfer simulations and realistic ocean and atmospheric fields, with the instrument specifications of CIMR (top) and of AMSR2 (bottom). SST = sea surface temperature; CIMR = Copernicus Imaging Microwave Radiometer; AMSR2 = Advanced Microwave Scanning Radiometer 2; StD = standard deviation.

0.125° spatial resolution. For SSS information at a global scale, we use the same MERCATOR product than previously in section 3.1. All the variables are reprojected on a grid of 0.05° spatial resolution.

Figure 12 presents the precision on the SST retrieval for CIMR and for AMSR2 missions at global scale. The distributions of the SST theoretical retrieval error StDs are indicated in Figure 13. With CIMR, the mode value of the distribution is at 0.2 K. For lower SST, the error can reach 0.45 K. Compared to the AMSR2 performances, this is an important improvement. Note that these results for AMSR2 are consistent with the validation of the AMSR SST products that showed mean errors of the order of 0.4 K as compared to buoys (Nielsen-Englyst et al., 2018; O'Carroll et al., 2008), suggesting that our method to evaluate the new CIMR mission is valid.

4. Discussion and Conclusions

A new satellite mission concept, CIMR, is currently being considered to estimate all weather and high spatial resolution ocean and sea ice surface parameters. It is a conically scanning passive microwave imager in a Sun-synchronous polar orbit, with a 7-m foldable antenna and low noise receivers. It observes at 1.4, 6.9, 10.65, 18.7, and 36.5 GHz, for both perpendicular polarizations. An information content analysis is conducted, for the retrieval of SST, SSS, and SIC. The precision for each product is estimated and compared to the precision achieved with the current instruments. With the CIMR mission, the retrieval error StDs are between 0.15 and 0.45 K for the SST, 0.2 and 0.6 psu for the SSS, and 2% and 5% for SIC. Estimation of global retrieval errors, based on realistic ocean and sea ice fields data revealed that SST will have an error StD mode value of 0.2 K, compared to 0.35 K with the current AMSR2 mission. The CIMR mission will provide SST information at closer than 30 km from the coasts compared to 100 km with AMSR2. In polar regions where SST and SSS retrievals are especially

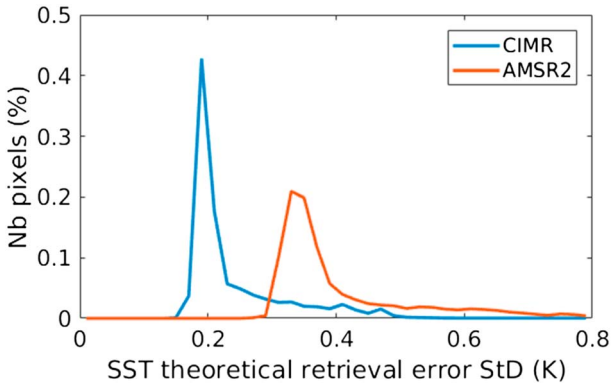

Figure 13. Histograms of the SST theoretical retrieval error StD for 1 day (15 June 2008) for CIMR and AMSR2 missions. SST = sea surface temperature; CIMR = Copernicus Imaging Microwave Radiometer; AMSR2 = Advanced Microwave Scanning Radiometer 2; StD = standard deviation.

difficult and where there are crucial issues for operational weather prediction and climate, CIMR will give a radiometric accuracy close to 0.4 K for SST and 0.6 psu for SSS, compared to 0.6 K and 0.9 psu, respectively, typical of the current generation of satellite microwave radiometers (for a given SST of 273 K and a given SSS of 35 psu). The spatial resolution of SIC products will be largely improved and 5-km spatial resolution possible from CIMR with a retrieval precision below 5% for most environments. Table 2 summarizes the performances of CIMR in terms of geophysical products.

The final definition of the CIMR characteristics will be the result of different trade-offs, in terms of spatial resolution and retrieval precision. Better spatial resolution could be achieved with a decrease of the incidence zenith angle. SMAP for instance observes with a 40° incidence angle. But for this geometry, the poles cannot be fully covered. The sensitivity to the SST decreases, and the retrieval precision would be significantly degraded, mainly due to the decreasing emissivity with decreasing incidence angle for the vertical polarization. In addition, the swath would be reduced, and as a consequence, the revisit cycle degraded. The complete coverage of the pole is a key issue for polar studies. Orbitography calculations with IXION (http://climserv.ipsl.polytechnique.fr/ixion/; Capderou, 2006) showed that an incidence angle of 55° with a Sun-synchronous orbit at 830-km altitude provides a full coverage of the pole.

Simultaneous measurements between 1.4 and 36.5 GHz (L, C, X, Ku, and Ka bands) mean that the CIMR mission will combine and build on the merits of heritage missions including AMSR and SMOS/SMAP-type missions. It will provide simultaneous and consistent retrievals of different parameters, needed for many applications and most importantly, addressing the Integrated European Union Strategy for the Arctic. For instance, with the SST and SSS controlling the density of the sea water (Boutin et al., 2016), twice daily accurate instantaneous estimate of SST and SSS will lead to an improved monitoring of sea surface density that may constrain air-sea exchanges (e.g., barrier layers). By the same token, the consistency between high-resolution SST and SIC measurements will also be a significant step forward for all applications addressing ocean/sea ice interactions in the marginal ice zone, with rigorous collocation and identical spatial/temporal sampling of the products, as compared to a multiplatform approach.

Table 2
Performances of a Potential Copernicus Imaging Microwave Radiometer Mission for the Retrieval of the Main Ocean and Sea-Ice Products

Parameter	Spatial resolution	Precision	Time sampling
SST	15 km	0.2 K	Twice daily
SSS	55 km	0.3 psu	Twice daily
SIC	5 km*	5%*	Twice daily

Note. SST = sea surface temperature; SSS = sea surface salinity; SIC = sea ice concentration.
*Preliminary results at 5 km. Work underway to consolidate these results. At 15-km resolution, the precision is below 3%.

In addition to the ocean and sea ice parameters already discussed, CIMR has the capability to provide other key surface information, over both ocean and sea ice. Under extreme conditions (e.g., high rain rate or hurricane), no wind information was available until recently. Reul et al. (2012) and Meissner et al. (2017) showed that surface wind information under extreme conditions could be derived from observations at 1.4 GHz with SMOS and SMAP, with strong interest for operational hurricane intensity forecast models. CIMR could benefit from this high wind speed capacity with its 1.4-GHz measurement, in addition to the estimates of lower wind speed thanks to the coupled observations between 6.9 and 36.5 GHz. Thickness of sea ice is required for sea ice modeling and operations. Ice thicknesses above ~1 m are estimated from radar altimetry (CryoSat2), but for the thinner and more vulnerable sea ice, only 1.4-GHz observations from SMOS and SMAP are currently providing information (e.g., Huntemann et al., 2014), and this could be continued with CIMR. The dual polarization and frequency combination from 1.4 to 36.5 GHz will also allow the retrieval of snow depth on sea ice, sea ice type, sea-ice drift, and snow-ice interface temperatures more reliably and with higher spatial resolution than with current methods. High spatial resolution and quality observations between 1.4 and 36.5 GHz observations will also serve the continental surface community for soil moisture, surface water, and vegetation applications, following the heritage of AMSR2 and SMOS/SMAP capabilities (e.g., Kerr et al., 2012; Y. Y. Liu et al., 2012; Parrens et al., 2017).

With no guarantee of successors to AMSR2, SMOS, and SMAP, the CIMR mission will provide continuity in the observations of low frequency microwave measurements, with much improved radiometric and/or spatial characteristics, for an all weather observations capability of key surface parameters, over all surface types. This new concept is therefore a serious candidate for a future Copernicus mission to provide evidence that underpins European policies and services. Such a capability has been discussed for many years and will be an essential asset to monitor the rapidly evolving state of the Arctic Ocean as sea ice coverage continues to decrease with associated risk of climate scale feedback mechanisms that have implications for global circulation in both the atmosphere and the ocean.

Acknowledgments
The authors express their thanks to the MICROWAT team for all the developments and discussions during the last years. This strongly consolidated the requirements for the CIMR mission. They are also grateful to the CIMR mission advisory group for numerous discussions on the CIMR mission requirements and possible exploitation. They thank the two anonymous reviewers for their careful reading of the manuscript and for their valuable suggestions. They thank the PNTS (Programme National de Télédétection Spatiale) for their support for this study. The users can access the data containing the outputs of the sea emissivity model following this link: https://www.dropbox.com/sh/9if3j2i9wty245b/AADm60GM8ImCvived2XJtSG_a?dl=0. The RRDP of the sea ice CCI project is available at http://www.seaice.dk/ecv2/rrdb-v1.1/.

References

Aires, F., Prigent, C., Bernardo, F., Jiménez, C., Saunders, R., & Brunel, P. (2011). A Tool to Estimate Land-Surface Emissivities at Microwave frequencies (TELSEM) for use in numerical weather prediction. *Quarterly Journal of the Royal Meteorological Society*, *137*(656), 690–699.

Bell, M. J., Forbes, R. M., & Hines, A. (2000). Assessment of the FOAM global data assimilation system for real-time operational ocean forecasting. *Journal of Marine Systems*, *25*(1), 1–22.

Boutin, J., Chao, Y., Asher, W. E., Delcroix, T., Drucker, R., Drushka, K., et al. (2016). Satellite and in situ salinity: Understanding near-surface stratification and subfootprint variability. *Bulletin of the American Meteorological Society*, *97*(8), 1391–1407.

Boutin, J., Vergely, J. L., Marchand, S., D'Amico, F., Hasson, A., Kolodziejczyk, N., et al. (2018). New SMOS sea surface salinity with reduced systematic errors and improved variability. *Remote Sensing of Environment*, *214*, 115–134.

Capderou, M. (2006). *Satellites: Orbits and missions*. Germany: Springer Science & Business Media.

Chelton, D. B., & Wentz, F. J. (2005). Global microwave satellite observations of sea surface temperature for numerical weather prediction and climate research. *Bulletin of the American Meteorological Society*, *86*(8), 1097–1115.

Chin, T. M., Vazquez-Cuervo, J., & Armstrong, E. M. (2017). A multi-scale high-resolution analysis of global sea surface temperature. *Remote Sensing of Environment*, *200*, 154–169.

Comiso, J. C., Cavalieri, D. J., Parkinson, C. L., & Gloersen, P. (1997). Passive microwave algorithms for sea ice concentration: A comparison of two techniques. *Remote Sensing of Environment*, *60*(3), 357–384.

Dinnat, E. P., Boutin, J., Caudal, G., & Etcheto, J. (2003). Issues concerning the sea emissivity modeling at L band for retrieving surface salinity. *Radio Science*, *38*(4), 8060. https://doi.org/10.1029/2002RS002637

Donlon, C. J. (2018). Copernicus Imaging Microwave Radiometer (CIMR) mission requirements document, version 1.5 (Tech. Rep.). Noordwijk, Netherlands: European Space Agency.

Donlon, C. J., Martin, M., Stark, J., Roberts-Jones, J., Fiedler, E., & Wimmer, W. (2012). The operational sea surface temperature and sea ice analysis (OSTIA) system. *Remote Sensing of Environment*, *116*, 140–158.

Duchossois, G., Strobl, P., Toumazou, V., Antunes, S., Bartsch, A., Diehl, T., et al. (2018a). User requirements for a Copernicus polar mission—Phase 2 report (Tech. Rep. No. 11068). Europe: EUR (29144) European Commission Joint Research Centre. https://doi.org/10.2760/44170

Duchossois, G., Strobl, P., Toumazou, V., Antunes, S., Bartsch, A., Diehl, T., et al. (2018b). User requirements for a Copernicus polar mission—Phase 1 report (Tech. Rep. No. 11067). Europe: EUR (29144) European Commission Joint Research Centre. https://doi.org/10.2760/22832

Durden, S. L., & Vesecky, J. F. (1985). A physical radar cross-section model for a wind-driven sea with swell. *IEEE Journal of Oceanic Engineering*, *10*(4), 445–451.

Eppler, D. T., Farmer, L. D., Lohanick, A. W., Anderson, M. R., Cavalieri, D. J., Comiso, J., et al. (1992). Passive microwave signatures of sea ice. In F. D. Carsey (Ed.), *Microwave remote sensing of sea ice* (pp. 47–71). Washington, DC: American Geophysical Union.

European Space Agency (2018). Copernicus Imaging Microwave Radiometer (CIMR) —Mission requirements document. EDSA-EOPSM-CIMR-MRD-3236, version 1.5, rev. 5

Fore, A. G., Yueh, S. H., Tang, W., Stiles, B. W., & Hayashi, A. K. (2016). Combined active/passive retrievals of ocean vector wind and sea surface salinity with SMAP. *IEEE Transactions on Geoscience and Remote Sensing*, *54*(12), 7396–7404.

Frenger, I., Gruber, N., Knutti, R., & Münnich, M. (2013). Imprint of Southern Ocean eddies on winds, clouds and rainfall. *Nature Geoscience*, *6*(8), 608–612.

Gabarro, C., Turiel, A., Elosegui, P., Pla-Resina, J. A., & Portabella, M. (2017). New methodology to estimate arctic sea ice concentration from SMOS combining brightness temperature differences in a maximum-likelihood estimator. *The Cryosphere*, *11*(4), 1987.
Gentemann, C. L., Meissner, T., & Wentz, F. J. (2010). Accuracy of satellite sea surface temperatures at 7 and 11 GHz. *IEEE Transactions on Geoscience and Remote Sensing*, *48*(3), 1009–1018.
Gloersen, P., Campbell, W. J., Cavalieri, D. J., Comiso, J. C., Parkinson, C. L., & Zwally, H. J. (1992). Arctic and Antarctic sea ice. *NASA-SP-511* (Vol. *290*, pp. 149–154).
Huntemann, M., Heygster, G., Kaleschke, L., Krumpen, T., Mäkynen, M., & Drusch, M. (2014). Empirical sea ice thickness retrieval during the freeze-up period from SMOS high incident angle observations. *The Cryosphere*, *8*(2), 439–451.
Imaoka, K., Kachi, M., Kasahara, M., Ito, N., Nakagawa, K., & Oki, T. (2010). Instrument performance and calibration of AMSR-E and AMSR2. *International Archives of the Photogrammetry, Remote Sensing and Spatial Information Science*, *38*(8), 13–18.
Ivanova, N., Pedersen, L. T., Tonboe, R. T., Kern, S., Heygster, G., Lavergne, T., et al. (2015). Inter-comparison and evaluation of sea ice algorithms: Towards further identification of challenges and optimal approach using passive microwave observations. *The Cryosphere*, *9*(5), 1797–1817.
Kao, H.-Y., Lagerloef, G. S. E., Lee, T., Melnichenko, O., Meissner, T., & Hacker, P. (2018). Assessment of Aquarius sea surface salinity. *Remote Sensing*, *10*(9), 1341.
Kerr, Y. H., Waldteufel, P., Richaume, P., Wigneron, J. P., Ferrazzoli, P., Mahmoodi, A., et al. (2012). The SMOS soil moisture retrieval algorithm. *IEEE Transactions on Geoscience and Remote Sensing*, *50*(5), 1384–1403.
Klein, L., & Swift, C. (1977). An improved model for the dielectric constant of sea water at microwave frequencies. *Oceanic Engineering, IEEE Journal of*, *2*(1), 104–111.
Lagerloef, G., Colomb, F. R., Le Vine, D., Wentz, F., Yueh, S., Ruf, C., et al. (2008). The Aquarius/SAC-D mission: Designed to meet the salinity remote-sensing challenge. *Oceanography*, *21*, 68–81.
Le Vine, D. M., Dinnat, E. P., Meissner, T., Yueh, S. H., Wentz, F. J., Torrusio, S. E., & Lagerloef, G. (2015). Status of Aquarius/SAC-D and Aquarius salinity retrievals. *IEEE Journal of Selected Topics in Applied Earth Observations and Remote Sensing*, *8*(12), 5401–5415.
Liu, Y. Y., Dorigo, W. A., Parinussa, R. M., de Jeu, R. A. M., Wagner, W., McCabe, M. F., et al. (2012). Trend-preserving blending of passive and active microwave soil moisture retrievals. *Remote Sensing of Environment*, *123*, 280–297.
Liu, Q., Weng, F., & English, S. J. (2011). An improved fast microwave water emissivity model. *IEEE Transactions on Geoscience and Remote Sensing*, *49*(4), 1238–1250.
Markus, T., & Cavalieri, D. J. (2000). An enhancement of the NASA team sea ice algorithm. *IEEE Transactions on Geoscience and Remote Sensing*, *38*(3), 1387–1398.
Markus, T., & Cavalieri, D. J. (2004). AMSR-E algorithm theoretical basis document: Sea ice products (Tech. Rep. No. MD 20771). Center Greenbelt: Hydrospheric and Biospheric Sciences Laboratory, NASA Goddard Space Flight.
Meissner, T., Ricciardulli, L., & Wentz, F. J. (2017). Capability of the SMAP mission to measure ocean surface winds in storms. *Bulletin of the American Meteorological Society*, *98*(8), 1660–1677.
Meissner, T., Wentz, F. J., & Le Vine, D. M. (2018). The salinity retrieval algorithms for the NASA Aquarius version 5 and SMAP version 3 releases. *Remote Sensing*, *10*(7), 1121.
Meissner, T., Wentz, F. J., Scott, J., & Vazquez-Cuervo, J. (2016). Sensitivity of ocean surface salinity measurements from spaceborne L-band radiometers to ancillary sea surface temperature. *IEEE Transactions on Geoscience and Remote Sensing*, *54*(12), 7105–7111.
Nielsen-Englyst, P., Høyer, J., Toudal Pedersen, L., Gentemann, C., Alerskans, E., Block, T., & Donlon, C. (2018). Optimal estimation of sea surface temperature from AMSR-E. *Remote Sensing*, *10*(2), 229.
O'Carroll, A. G., Eyre, J. R., & Saunders, R. W. (2008). Three-way error analysis between AATSR, AMSR-E, and in situ sea surface temperature observations. *Journal of Atmospheric and Oceanic Technology*, *25*(7), 1197–1207.
Orlhac, J.-C. (2012). MICROWAT ESA final report (Tech. Rep. No. 739 EF.RP.JCO.12.00081). Toulouse, France: EADS Astrium.
Parrens, M., Wigneron, J.-P., Richaume, P., Al Bitar, A., Mialon, A., Fernandez-Moran, R., et al. (2017). Considering combined or separated roughness and vegetation effects in soil moisture retrievals. *International Journal of Applied Earth Observation and Geoinformation*, *55*, 73–86.
Pearson, K., Merchant, C., Embury, O., & Donlon, C. (2018). The role of advanced microwave scanning radiometer 2 channels within an optimal estimation scheme for sea surface temperature. *Remote Sensing*, *10*(1), 90.
Pedersen, L. F., & Saldo, R. (2016). Sea ice concentration (SIC) round robin data package, sea ice climate initiative: Phase 2 (Tech. Rep. No. SICCI-RRDP-07-16 Version: 1.4). DTU: ESA.
Perlin, N., de Szoeke, S. P., Chelton, D. B., Samelson, R. M., Skyllingstad, E. D., & O'Neill, L. W. (2014). Modeling the atmospheric boundary layer wind response to mesoscale sea surface temperature perturbations. *Monthly Weather Review*, *142*(11), 4284–4307.
Prigent, C., Aires, F., Bernardo, F., Orlhac, J.-C., Goutoule, J.-M., Roquet, H., & Donlon, C. (2013). Analysis of the potential and limitations of microwave radiometry for the retrieval of sea surface temperature: Definition of MICROWAT, a new mission concept. *Journal of Geophysical Research: Oceans*, *118*, 3074–3086. https://doi.org/10.1002/jgrc.20222
Prigent, C., Aires, F., & Rossow, W. B. (2006). Land surface microwave emissivities over the globe for a decade. *Bulletin of the American Meteorological Society*, *87*(11), 1573–1584.
Quilfen, Y., Prigent, C., Chapron, B., Mouche, A. A., & Houti, N. (2007). The potential of QuikSCAT and WindSat observations for the estimation of sea surface wind vector under severe weather conditions. *Journal of Geophysical Research*, *112*, C09023. https://doi.org/10.1029/2007JC004163
Reul, N., Chapron, B., Zabolotskikh, E., Donlon, C., Mouche, A., Tenerelli, J., et al. (2017). A new generation of tropical cyclone size measurements from space. *Bulletin of the American Meteorological Society*, *98*(11), 2367–2385.
Reul, N., Fournier, S., Boutin, J., Hernandez, O., Maes, C., Chapron, B., et al. (2014). Sea surface salinity observations from space with the SMOS satellite: A new means to monitor the marine branch of the water cycle. *Surveys in Geophysics*, *35*(3), 681–722.
Reul, N., Tenerelli, J., Chapron, B., Vandemark, D., Quilfen, Y., & Kerr, Y. (2012). SMOS satellite L-band radiometer: A new capability for ocean surface remote sensing in hurricanes. *Journal of Geophysical Research*, *117*, C02006. https://doi.org/10.1029/2011JC007474
Reul, N., Tenerelli, J. E., Floury, N., & Chapron, B. (2008). Earth-viewing L-band radiometer sensing of sea surface scattered celestial sky radiation; part II: Application to SMOS. *IEEE Transactions on Geoscience and Remote Sensing*, *46*(3), 675–688.
Rodgers, C. D. (1976). Retrieval of atmospheric temperature and composition from remote measurements of thermal radiation. *Reviews of Geophysics*, *14*(4), 609.
Rodgers, C. D. (1990). Characterization and error analysis of profiles retrieved from remote sounding measurements. *Journal of Geophysical Research*, *95*(D5), 5587.
Saunders, R., Matricardi, M., & Brunel, P. (1999). An improved fast radiative transfer model for assimilation of satellite radiance observations. *Quarterly Journal of the Royal Meteorological Society*, *125*(556), 1407–1425.

Schweiger, A. J. (2004). Changes in seasonal cloud cover over the Arctic seas from satellite and surface observations. *Geophysical Research Letters*, *31*, L12207. https://doi.org/10.1029/2004GL020067

Stark, J. D., Donlon, C. J., Martin, M. J., & McCulloch, M. E. (2007). OSTIA: An operational, high resolution, real time, global sea surface temperature analysis system. In *Oceans 2007-europe* (pp. 14). Aberdeen, UK.

Stocker, T. F., Qin, D., Plattner, G. K., Tignor, M., Allen, S. K., Boschung, J., et al. (2013). *IPCC, 2013: Climate change 2013: The physical science basis. Contribution of working group I to the fifth assessment report of the intergovernmental panel on climate change*. Cambridge, UK, and New York: Cambridge University Press.

Stogryn, A. (1971). Equations for calculating the dielectric constant of saline water (correspondence). *IEEE Transactions on Microwave Theory and Techniques*, *19*(8), 733–736.

Stogryn, A. (1972). The emissivity of sea foam at microwave frequencies. *Journal of Geophysical Research*, *77*(9), 1658–1666.

Tonboe, R, Andersen, S, Toudal, L, & Heygster, G (2006). Sea ice emission modelling applications. In C. Mätzler, P. W. Rosenkranz, A. Battaglia, & Wigneron, J. P. (Eds.), *Thermal microwave radiation-applications for remote sensing* (pp. 382–400). London, UK: IET Electromagnetic Waves Series.

Tonboe, R. T., Eastwood, S., Lavergne, T., Sørensen, A. M., Rathmann, N., Dybkjær, G., et al. (2016). The EUMETSAT sea ice climate record. *The Cryosphere*, *10*, 2275–2290.

Wentz, F. J., Gentemann, C., Smith, D., & Chelton, D. (2000). Satellite measurements of sea surface temperature through clouds. *Science*, *288*(5467), 847–850.

Wiesmann, A., & Mätzler, C. (1999). Microwave emission model of layered snowpacks. *Remote Sensing of Environment*, *70*(3), 307316.

Wilheit, T. T., & Chang, A. T. C. (1980). An algorithm for retrieval of ocean surface and atmospheric parameters from the observations of the scanning multichannel microwave radiometer. *Radio Science*, *15*(3), 525–544.

Winebrenner, D. P., Bredow, J., Fung, A. K., Drinkwater, M. R., Nghiem, S., Gow, A. J., et al. (1992). Microwave sea ice signature modeling. In F. D. Carsey (Ed.), *Microwave remote sensing of sea ice* (pp. 137–175). Washington, DC: American Geophysical Union.

Yin, X., Boutin, J., Martin, N., & Spurgeon, P. (2012). Optimization of L-band sea surface emissivity models deduced from SMOS data. *IEEE Transactions on Geoscience and Remote Sensing*, *50*(5), 1414–1426.

Yueh, S. H. (1997). Modeling of wind direction signals in polarimetric sea surface brightness temperatures. *IEEE Transactions on Geoscience and Remote Sensing*, *35*(6), 1400–1418.